

Kinetic symmetry energy of nucleonic matter with tensor correlations

Or Hen,^{1,*} Bao-An Li,² Wen-Jun Guo,^{2,3} L.B. Weinstein,⁴ and Eli Piasetzky¹

¹*School of Physics and Astronomy, Tel Aviv University, Tel Aviv 69978, Israel*

²*Department of Physics and Astronomy, Texas A&M University-Commerce, Commerce, TX 75429-3011, USA*

³*College of Science, University of Shanghai for Science and Technology, Shanghai, 200093, China*

⁴*Old Dominion University, Norfolk, VA 23529, USA*

(Dated: May 15, 2022)

The nuclear symmetry energy is a vital ingredient of our understanding of many processes, from heavy-ion collisions to neutron stars. While the total nuclear symmetry energy at nuclear saturation density (ρ_0) is relatively well determined, its decomposition into kinetic and potential parts is not. The kinetic symmetry energy, $E_{sym}^{kin}(\rho_0)$, equals the difference in the per-nucleon kinetic energy between pure neutron matter (PNM) and symmetric nuclear matter (SNM). This is often calculated in a simple Fermi gas model. However, experiments show that about 20% of nucleons in nuclei belong to high-momentum correlated pairs. Short-range correlations (SRC) due to the tensor force acting predominantly on neutron-proton pairs shift nucleons to high momentum in SNM where there are equal numbers of neutrons and protons, but have almost no effect in PNM. Using experimentally-derived correlated momentum distributions, we present an approximate analytical expression for $E_{sym}^{kin}(\rho_0)$ of correlated nucleonic matter. We further constrain our model with data on free neutron/proton ratios measured recently in intermediate energy nucleus-nucleus collisions to obtain $E_{sym}^{kin}(\rho_0) = -3.8 \pm 0.7$ MeV. This result agrees qualitatively with microscopic many-body calculations and differs significantly from the 12.5 MeV obtained for a free Fermi gas with no correlation. We also present an approximate analytical expression for the kinetic symmetry energy of correlated nucleonic matter as a function of nuclear density, $E_{sym}^{kin}(\rho)$.

PACS numbers: 25.70.-z, 25.60.-t, 25.80.Ls, 24.10.Lx

The nuclear symmetry energy $E_{sym}(\rho)$, where ρ is the nuclear density, is related to the difference in the energy per nucleon of pure neutron matter (PNM) and symmetric nuclear matter (SNM). It determines many nuclear and astrophysical properties, such as the cooling of proto-neutron stars [1], the mass-radius relations of neutron stars [2], properties of nuclei involved in r -process nucleosynthesis [3], and heavy-ion collisions [4–6].

Significant progress has been made in recent years in constraining $E_{sym}(\rho)$ especially around $\rho \approx \rho_0$, the saturation density, using data from both terrestrial laboratory experiments and astrophysical observations [7–12]. One recent survey found that the mean values of the symmetry energy at ρ_0 from 28 different model analyses of various data are all consistent with $E_{sym}(\rho_0) = 31.6 \pm 2.66$ MeV [13]. However, the decomposition of the symmetry energy into its kinetic and potential parts and its behavior at both sub-saturation ($\rho < \rho_0$) and supra-saturation ($\rho > \rho_0$) densities are still poorly known.

Much effort is being invested in improving our knowledge of $E_{sym}(\rho)$. In particular, several major radioactive beam facilities being built around the world have all listed constraining the symmetry energy as one of their major science drivers, see, e.g., Ref. [14]. Moreover, observations of neutron stars from current missions such as the Chandra X-ray and XMM-Newton observatories, and upcoming missions such as the Neutron star Interior Composition Explorer (NICER) [15] will provide high precision data to infer more accurately neutron star radii which are very sensitive to the symmetry energy [16–19]

We can improve our knowledge of $E_{sym}(\rho)$ by subdividing it into its potential and kinetic parts,

$$E_{sym}(\rho) = E_{sym}^{kin}(\rho) + E_{sym}^{pot}(\rho) \quad (1)$$

and probing them separately. The kinetic part can be readily calculated from the nuclear momentum distribution. The potential part is much less well understood, but can be determined by analyzing isovector observables in nuclear structures and reactions.

The kinetic part is often approximated in a nonrelativistic free Fermi gas model as the per-nucleon difference between the kinetic energy of pure neutron matter at a density ρ and the kinetic energy of symmetric nuclear matter where the protons and neutrons each have density $\rho/2$:

$$E_{sym}^{kin}(\rho)|_{FG} = (2^{\frac{2}{3}} - 1) \frac{3}{5} E_F(\rho) \approx 12.5 \text{ MeV} (\rho/\rho_0)^{2/3} \quad (2)$$

where $E_F(\rho)$ is the Fermi energy at density ρ .

However, short-range correlations (SRC) due to the tensor force acting predominantly between neutron-proton pairs significantly increase the average momentum and hence the kinetic energy in SNM but have almost no effect in PNM. They thus reduce significantly the kinetic symmetry energy, possibly even to negative values. This has been shown recently in both phenomenological models [20] and microscopic many-body theories [21–24]. For a given symmetry energy, $E_{sym}(\rho)$, the SRC induced decrease of $E_{sym}^{kin}(\rho)$ increases $E_{sym}^{pot}(\rho)$ beyond its Fermi Gas model limit of $E_{sym}^{pot}(\rho_0) = E_{sym}(\rho_0) -$

$E_{sym}^{kin}(\rho_0)|_{FG} \approx 19.1$ MeV at saturation density. This is important for transport model simulations of heavy-ion collisions [4–6, 25, 26].

In this Letter we provide an analytical expression for the kinetic symmetry energy of correlated nucleonic matter based on data at saturation density (ρ_0) from inclusive (e, e') and exclusive ($e, e'pN$) scattering experiments at the Thomas Jefferson National Accelerator Facility (JLab) [27–30, 41]. We further constrain our model using transport model analyses of nucleon emission data in intermediate energy heavy-ion collisions at Michigan State University (MSU) [31, 32].

It has long been known that the tensor force induced SRC leads to a high-momentum tail in the single-nucleon momentum distribution around 300–600 MeV/c [33, 34]. This high-momentum tail scales, i.e., its shape is almost identical for all nuclei from deuteron to infinite nuclear matter, see, e.g. Refs. [35–37]. The ratio of the momentum distribution in nucleus A to the deuteron for $300 \leq k \leq 600$ MeV/c, $a_2(A)$, equals the ratio of the per nucleon inclusive (e, e') cross sections for nucleus A to the deuteron for Bjorken scaling parameter x_B between about 1.5 and 1.9 [27–29]. Extrapolation of the measured $a_2(A)$ to infinite SNM, based on correlation with the average removal energy of nucleons in nuclei and SNM, yield a value of $a_2(\infty) = 6.5 \pm 1.0$ [38, 39].

Exclusive two-nucleon knockout experiments [40–43] show that, for $300 \leq k \leq 600$ MeV/c, proton knockout is accompanied by a recoil second nucleon and that second nucleon is predominantly a neutron, i.e., that np -SRC pairs dominate over pp pairs by a factor of about 20. For recent reviews, see Refs. [44, 45]. This implies that correlations are about 20 times smaller in PNM than in SNM. Since the integral of the deuteron momentum distribution from 300 to 600 MeV/c is about 4% [46] and $a_2(\infty) = 6.5 \pm 1.0$, the probability to find a high-momentum nucleon in SNM is about 25% and in PNM is about 1–2%.

It was recently pointed out that the nuclear momentum distribution, $n_A(k)$, decreases as $1/k^4$ for $300 \leq k \leq 600$ MeV/c, or that $n_A(k/k_F)(k/k_F)^4 = R_d a_2(A)$ [47], where $R_d = 0.64 \pm 0.10$ is extracted from the deuteron momentum distribution, and k_F is the Fermi momentum [47]. At higher momenta, the momentum distribution $n(k)$ drops much more rapidly.

We therefore model $n(k)$ for SNM with a depleted Fermi gas region and a correlated high-momentum tail:

$$n_{SNM}^{SRC}(k) = \begin{cases} A_0 & k < k_F \\ C_\infty/k^4 & k_F < k < \lambda k_F^0 \\ 0 & k > \lambda k_F^0 \end{cases} \quad (3)$$

where $C_\infty = R_d \cdot a_2(\infty) \cdot k_F \equiv c_0 \cdot k_F$ is the phenomenological factor [47], $c_0 = 4.16 \pm 0.95$, k_F^0 is the Fermi momentum at ρ_0 and $\lambda \approx 2.75 \pm 0.25$ is the high-momentum cutoff obtained from the momentum distribution of the

deuteron [47]. A_0 is a constant given by

$$A_0 = \frac{3\pi^2}{(k_F^0)^3} \frac{\rho_0}{\rho} \left[1 - \left[1 - \frac{1}{\lambda} \left(\frac{\rho}{\rho_0} \right)^{1/3} \right] \frac{c_0}{\pi^2} \right], \quad (4)$$

determined by the normalization

$$\frac{4\pi}{(2\pi)^3} \int_0^{\lambda k_F^0} 2n_{SNM}^{SRC}(k) \cdot k^2 \cdot dk \equiv 1. \quad (5)$$

Based on the JLab data [41], fewer than 2% of neutrons belong to nn -SRC pairs. We thus use the free Fermi gas model for PNM and include the 2% upper limit for correlated neutrons in our estimate of the uncertainty band. In what follows we refer to this as the Correlated Fermi Gas (CFG) model.

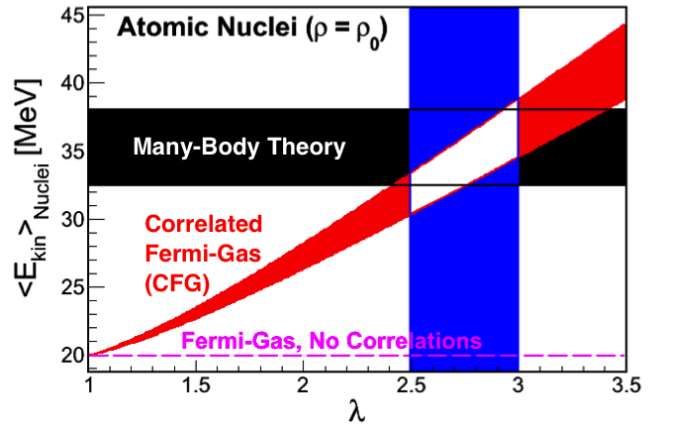


FIG. 1: (Color online) The per-nucleon kinetic energy calculated using the Correlated Fermi Gas (CFG) model (red band) for atomic nuclei from ^{12}C to ^{208}Pb . The calculated kinetic energy is shown as a function of λ , the high-momentum tail cutoff parameter. The blue band shows the constraints on λ from the deuteron momentum distribution. The red band reflects the model uncertainties. Also shown are the results from the uncorrelated Fermi Gas model (dashed purple line) and a black band spanning the results from many-body nuclear calculations for various nuclei from ^{12}C to ^{208}Pb [48] and from exact variational Monte Carlo (VMC) calculations for ^{12}C [49].

The per nucleon kinetic energy of nuclei and of symmetric nuclear matter can then be calculated from the momentum distribution using

$$E_{kin} = \int_0^\infty \frac{\hbar^2 k^2}{2m} n(k) k^2 dk. \quad (6)$$

Fig. 1 shows the resulting kinetic energy for finite nuclei, calculated within the CFG model using $a_2(A) = 5 \pm 0.3$. The CFG kinetic energy is much larger than that of the uncorrelated Fermi Gas. It agrees with the kinetic energies from many-body nuclear calculations for ^{12}C , ^{16}O , ^{40}Ca , ^{56}Fe , and ^{208}Pb [48] and from ‘exact’ variational Monte Carlo (VMC) calculations for ^{12}C [49].

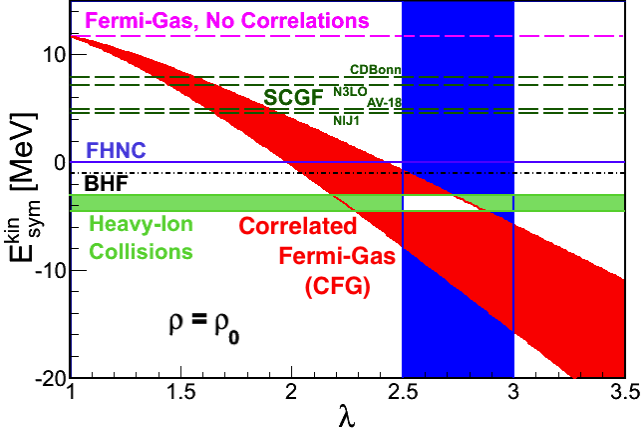


FIG. 2: (Color online) The per-nucleon kinetic symmetry energy at saturation density, $E_{sym}^{kin}(\rho_0)$, calculated using the Correlated Fermi-Gas model (red band) as a function of λ , the high-momentum tail cutoff parameter. The (dashed purple line) shows the results of the uncorrelated Fermi Gas model. The green band shows the results from transport model analyses of Sn+Sn collisions described in the text. Also shown for comparison are the results from microscopic calculations: Brueckner-Hartree-Fock (BHF) [21], Fermi-Hyper-Netted-Chain (FHNC) [22] and the Self-Consistent Greens Function (SCGF) using the CDBonn, N3LO, and AV18 interactions [23, 24].

Almost all phenomenological and microscopic many-body theories lead to Equations of State (EOS) of asymmetric nucleonic matter that vary quadratically with the isospin-asymmetry $\delta = (\rho_n - \rho_p)/(\rho_n + \rho_p)$ according to the so-called empirical parabolic law $E(\rho, \delta) = E(\rho, \delta = 0) + E_{sym}(\rho)\delta^2 + O(\delta^4)$. The coefficient of the δ^4 term at ρ_0 has been found to be less than 1 MeV [26]. The symmetry energy can thus be calculated equally accurately from either the energy difference between PNM and SNM, i.e., $E_{sym}(\rho) = E(\rho, 1) - E(\rho, 0)$ or the curvature $E_{sym}(\rho) = \frac{1}{2} \frac{\partial^2 E(\rho, \delta)}{\partial \delta^2}$ at any δ .

However, it has never been tested whether the empirical parabolic law is valid separately for the kinetic and potential parts of the EOS. While the free Fermi gas kinetic energy satisfies the parabolic law, models that include SRC not necessarily do so [51]. To be consistent and compare with the free Fermi gas model and microscopic many-body theories, we will define the kinetic symmetry energy of correlated nucleonic matter as $E_{sym}^{kin}(\rho) = E_{PNM}^{kin}(\rho) - E_{SNM}^{kin}(\rho)$. We add a SRC correction term to the Fermi Gas symmetry energy to get the full kinetic symmetry energy:

$$E_{sym}^{kin}(\rho) = E_{sym}^{kin}(\rho)|_{FG} - \Delta E_{sym}^{kin}(\rho) \quad (7)$$

where the SRC correction term is:

$$\Delta E_{sym}^{kin} \equiv \frac{E_F^0}{\pi^2} c_0 \left[\lambda \left(\frac{\rho}{\rho_0} \right)^{1/3} - \frac{8}{5} \left(\frac{\rho}{\rho_0} \right)^{2/3} + \frac{3}{5} \frac{1}{\lambda} \left(\frac{\rho}{\rho_0} \right) \right]. \quad (8)$$

As one expects, the SRC correction increases with both the height ($c_0 = C_\infty/k_F = R_d a_2(\infty)$) and width (λ) of the high-momentum tail in SNM.

Fig. 2 shows the kinetic symmetry energy $E_{sym}^{kin}(\rho_0)$ of correlated nucleonic matter at saturation density as a function of λ in comparison with the predictions of several microscopic models [21–24] and the free Fermi gas model. The error band of $E_{sym}^{kin}(\rho_0)$ combines estimated uncertainties in $R_d, a_2(\infty)$ and the amount of SRC in PNM. Within the uncertainty range of the parameter $\lambda = 2.75 \pm 0.25$ (blue band), $E_{sym}^{kin}(\rho_0)$ is found to be around -9 ± 7 MeV which is much less than the free Fermi gas result of $\approx +12.5$ MeV. The microscopic many-body theories yield results that are significantly smaller than our CFG model. The self-consistent Green's function (SCGF) calculations of the kinetic energy of symmetric nuclear matter, $E_{SNM}^{kin}(\rho_0)$, agree with our CFG calculation (see Fig. S1 in the supplemental material). However, the SCGF symmetry energy, $E_{sym}^{kin}(\rho_0) = E_{PNM}^{kin}(\rho_0) - E_{SNM}^{kin}(\rho_0)$, is significantly larger. This is because while they include about 20% correlations in SNM, they also include approximately 10% correlations in PNM.

The dynamics of heavy-ion collisions around the Fermi energy are sensitive to the density dependence of the nuclear symmetry energy around ρ_0 [25, 26]. The ratio of free neutrons to protons emitted in heavy-ion collisions was found to be the most sensitive and direct observable [4] for probing the symmetry energy. This ratio has been measured recently in $^{124}\text{Sn} + ^{124}\text{Sn}$ and $^{112}\text{Sn} + ^{112}\text{Sn}$ reactions at $E_{beam}/A = 50$ and 120 MeV at MSU [32] with much better precision than earlier experiments [31]. The data are given for the double ratio of neutrons to protons in $^{124}\text{Sn} + ^{124}\text{Sn}$ to $^{112}\text{Sn} + ^{112}\text{Sn}$ reactions to reduce systematic errors associated with neutron detection.

We performed an IBUU transport model [26] analysis of this double ratio by introducing two parameters, η and γ , in modeling the potential symmetry energy

$$E_{sym}^{pot}(\rho) = [E_{sym}(\rho_0) - \eta \cdot E_{sym}^{kin}(\rho_0)|_{FG}] \cdot (\rho/\rho_0)^\gamma. \quad (9)$$

Without considering the momentum dependence of nuclear potentials, the corresponding symmetry potential is then

$$V_{sym}^{n/p}(\rho, \delta) = [E_{sym}(\rho_0) - \eta \cdot E_{sym}^{kin}(\rho_0)|_{FG}] (\rho/\rho_0)^\gamma \times [\pm 2\delta + (\gamma - 1)\delta^2]. \quad (10)$$

The 2δ term dominates. The \pm sign is due to the fact that neutrons and protons feel repulsive and attractive symmetry potentials respectively.

We varied η and γ on a large 2D fine lattice to minimize the χ^2 between the model calculations and the MSU data at both beam energies. We then performed a covariance analysis to find the uncertainties of η and γ corresponding to a $\pm 1\sigma$ error band using the method reviewed recently

in Refs. [52, 53]. We used an impact parameter of 3 fm, consistent with that estimated for the data [54]. Free nucleons are identified as those with local densities less than $\rho_0/8$ at the time of their final freeze-out from the reaction. Calculations using a phase-space coalescence model lead to similar results within the error band [55].

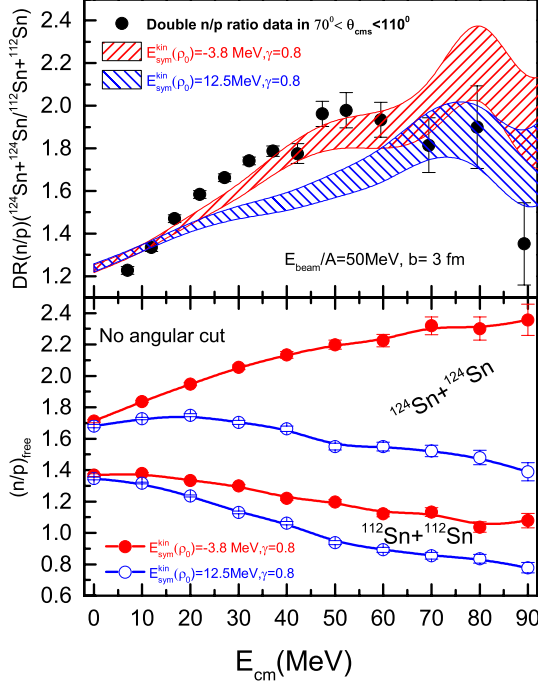


FIG. 3: (Color online) (Lower window) The calculated free neutron/proton ratio in $^{124}\text{Sn}+^{124}\text{Sn}$ and $^{112}\text{Sn}+^{112}\text{Sn}$ reactions in full phase space at $E_{beam}/A = 50$ MeV and an impact parameter of 3 fm. (Upper window) The calculated double ratio of free neutron/protons in the two reactions in comparison with the MSU data for transversely emitted nucleons in the angular range of $70^\circ \leq \theta_{cms} \leq 110^\circ$ [32]. The bands represent 1σ uncertainty of the calculations.

Fig. 3 shows the single (lower panel) and double (upper panel) free neutron/proton ratios in the two Sn+Sn reactions at $E_{beam}/A = 50$ MeV/nucleon [32]. The calculations (red band) shown used the optimized parameters $\eta_0 = -0.30(1 \pm 18.53\%)$ and $\gamma_0 = 0.80(1 \pm 5.98\%)$ with a $\chi^2_0 = 8$. The $\eta_0 = -0.30(1 \pm 18.5\%)$ corresponds to $E_{sym}^{kin}(\rho_0) = -(3.8 \pm 0.7)$ MeV. This value of $E_{sym}^{kin}(\rho_0)$ was determined without considering the momentum dependence of the symmetry potential known to decrease somewhat the free neutron/proton ratio [56]. It thus represents the maximum kinetic symmetry energy allowed to reproduce the MSU data. For comparison, results with a $\chi^2 = 21$ using $E_{sym}^{kin}(\rho_0)|_{FG} = 12.5$ MeV and $\gamma = 0.8$

are also shown. Calculations with $E_{sym}^{kin}(\rho_0)|_{FG}$ and other values of γ between 0.4 and 1 leads to higher χ^2 values.

To understand effects of the reduced $E_{sym}^{kin}(\rho_0)$ it is instructive to also examine the single neutron/proton ratio in each reaction. The lower panel of Fig. 3 shows that the reduced kinetic symmetry energy at $\rho = \rho_0$ increases the potential symmetry energy which leads to an enhanced neutron to proton ratio for both reactions because of the stronger repulsive (attractive) symmetry potential for neutrons (protons). The effect is more pronounced for more energetic nucleons as they are the ones mostly from the participant region in the earlier stage of the reaction where the nucleon density is higher.

Measurements at $E_{beam}/A = 120$ MeV are even better described by the calculation [55] but have reduced sensitivity to the symmetry energy. The reduced sensitivity to the symmetry energy at higher beam energies is due to the increased effects of nucleon-nucleon collisions over the mean-field in the reaction dynamics and the decreased ratio of isovector/isoscalar potential at higher densities [26].

The value of $E_{sym}^{kin}(\rho_0)$ determined from the neutron to proton ratios in Sn+Sn collisions is consistent with that calculated using our CFG model (see Fig. 2). By combining the Sn+Sn collision value of $E_{sym}^{kin}(\rho_0) = -3.8 \pm 0.7$ MeV with the electron scattering data, we can further restrict the height and width parameters of the CFG model to $\lambda = 2.7 \pm 0.2$ and $c_0 = 3.7 \pm 0.5$ (see Fig. S2 in the supplemental material). Using Eq. 7 we can also predict the density dependence of the kinetic symmetry energy. For $0.5 \leq \rho/\rho_0 \leq 3$, $E_{sym}^{kin}(\rho)$ in the CFG model has the same slope as the free Fermi gas model but with significantly reduced value.

To summarize, while the electron scattering and nucleus-nucleus collision experiments probe directly the kinetic and potential symmetry energies respectively, they are interconnected. Synthesizing complementary information from these experiments we provided an analytical expression for a negative kinetic symmetry energy of correlated nucleonic matter at $\rho = \rho_0$ in contrast to the free Fermi gas model prediction widely used in nuclear physics and astrophysics over the last several decades.

We would like to thank F.J. Fattoyev, X. H. Li, W.G. Newton, Z.Z. Shi, A. Gal, M. M. Sargsian, G. A. Miller, D. W. Higinbotham, M. Strikman, and L. Frankfurt for helpful discussions. O. Hen and E. Piasetzky are supported by the Israel Science Foundation. B.A. Li is supported in part by the US National Science Foundation under Grant No. PHY-1068022, US National Aeronautics and Space Administration under Grant No. NNX11AC41G issued through the Science Mission Directorate, the CUSTIPEN (China-U.S. Theory Institute for Physics with Exotic Nuclei) under DOE grant number DE-FG02-13ER42025 and the National Natural Science Foundation of China under Grant No. 11320101004. W.J. Guo is supported by the National Natural Science

Foundation of China (10905041) and the China Scholarship Council Foundation (201208310156). L. B. Weinstein is supported by US Department of Energy under Grants xxx and xxx.

* Contact Author or.chen@mail.huji.ac.il

- [1] J.M. Lattimer, C.J. Pethick, M. Prakash, P. Haensel, *Phys. Rev. Lett.* **66**, 2701 (1991).
- [2] M. Prakash, T.L. Ainsworth, J.M. Lattimer, *Phys. Rev. Lett.* **61**, 2518 (1988).
- [3] N. Nikolov, N. Schunck, W. Nazarewicz, M. Bender, and J. Pei, *Phys. Rev. C* **83**, 034305 (2011).
- [4] B.A. Li, C.M. Ko, Z.Z. Ren, *Phys. Rev. Lett.* **78**, 1644 (1997).
- [5] L.W. Chen, C.M. Ko, B.A. Li, *Phys. Rev. Lett.* **94**, 032701 (2005).
- [6] M.B. Tsang et al., *Phys. Rev. Lett.* **102**, 122701, (2009).
- [7] W.G. Lynch et al., *Prog. Nucl. Part. Phys.* **62**, 427 (2009).
- [8] W. Trautmann and H. H. Wolter, *Int. J. Mod. Phys. E* **21**, 1230003 (2012).
- [9] M. B. Tsang, et al., *Phys. Rev. C* **86**, 015803 (2012).
- [10] B.A. Li, A. Ramos, G. Verde, and I. Vidaña, eds., "Topical issue on nuclear symmetry energy", *Eur. Phys. J. A* **50**, No. 2, (2014).
- [11] C.J. Horowitz et al., *J. of Phys. G* **41**, 093001 (2014).
- [12] J. M. Lattimer, *Annu. Rev. Nucl. Part. Sci.* **62**, 485 (2012).
- [13] B.A. Li, X. Han, *Phys. Lett. B* **727**, 276 (2013).
- [14] A. B. Balantekin et al., *Modern Physics Letters A*, **29**, 30010 (2014).
- [15] C. Kouveliotou et al., *Enduring Quests-Daring Visions (NASA Astrophysics in the Next Three Decades)*. ArXiv e-prints, January 2014.
- [16] A.W. Steiner, M. Prakash, J.M. Lattimer, P.J. Ellis, *Phys. Rep.* **411**, 325 (2005).
- [17] B. A. Li and A. W. Steiner, *Phys. Lett. B* **642**, 436 (2006).
- [18] A. W. Steiner, J. M. Lattimer, and E. F. Brown, *Astrophys. J.* **722**, 33 (2010).
- [19] W.G. Newton, M. Gearheart and B.A. Li, *APJ Supplementary Series* **204**, 9 (2013).
- [20] C. Xu and B.A. Li, arXiv: 1104.2075; C. Xu, A. Li, B.A. Li, *J. of Phys. Conference Series* **420**, 012190 (2013).
- [21] I. Vidana, A. Polls, C. Providencia, *Phys Rev C* **84**, 062801(R) (2011).
- [22] A. Lovato, O. Benhar, S. Fantoni, A. Yu. Illarionov, and K. E. Schmidt, *Phys. Rev. C* **83**, 054003 (2011).
- [23] A. Carbone, A. Polls, A. Rios, *Eur. Phys. Lett.* **97**, 22001 (2012).
- [24] A. Rios, A. Polls, W. H. Dickhoff, *Phys. Rev. C* **89**, 044303 (2014).
- [25] V. Baran, M. Colonna, V. Greco, and M. Di Toro, *Phys. Rep.* **410**, 335 (2005).
- [26] B. A. Li, L. W. Chen, and C. M. Ko, *Phys. Rep.* **464**, 113 (2008).
- [27] K. Egiyan, et al. (The CLAS Collaboration), *Phys. Rev. C* **68**, 014313 (2003).
- [28] K. Egiyan, et al. (The CLAS Collaboration), *Phys. Rev. Lett.* **96**, 082501 (2006).
- [29] N. Fomin, et al. (The Hall C Collaboration), *Phys. Rev. Lett.* **108**, 092502 (2012).
- [30] O. Hen et al. (The CLAS Collaboration), submitted for publication (2014).
- [31] M.A. Famiano et al., *Phys. Rev. Lett.* **97**, 052701 (2006).
- [32] D.S. Coupland et al., arXiv:1406.4546
- [33] H.A. Bethe, *Ann. Rev. Nucl. Part. Sci.* **21**, 93 (1971).
- [34] A.N. Antonov, P.E. Hodgson and I.Z. Petkov, *Nucleon Momentum and Density Distributions in Nuclei* (Clarendon Press, Oxford, 1988).
- [35] S. Fantoni and V.R. Pandharipande, *Nucl. Phys. A* **427**, 473 (1984).
- [36] S.C. Pieper, R.B. Wiringa and V.R. Pandharipande, *Phys. Rev. C* **46**, 1741 (1992).
- [37] C. Ciofi degli Atti and S. Simula, *Phys. Rev. C* **53**, 1689 (1996).
- [38] E. Piasetzky, O. Hen, and L. B. Weinstein, *AIP Conf. Proc.* **1560**, 355 (2013).
- [39] O. Benhar and I. Sick, arXiv: 1207.4595 (2012).
- [40] E. Piasetzky et al., *Phys. Rev. Lett.* **97**, 162504 (2006).
- [41] R. Subedi, et al. (The Hall A Collaboration), *Science* **320**, 1476 (2008).
- [42] A. Tang et al., *Phys. Rev. Lett.* **90**, 042301 (2003).
- [43] H. Baghdasaryan, et al. (The CLAS Collaboration), *Phys. Rev. Lett.* **105**, 222501 (2010).
- [44] L. Frankfurt, M. Sargsian and M. Strikman, *Int. Jour. Mod. Phys. A* **23**, 2991 (2008).
- [45] J. Arrington, D.W. Higinbotham, G. Rosner G and M. Sargsian, *Prog. Part. Nucl. Phys.* **67**, 898 (2012).
- [46] I. Passchier et al., *Phys. Rev. Lett.* **88**, 102302 (2002).
- [47] O. Hen, L. B. Weinstein, E. Piasetzky, G. A. Miller, M. M. Sargsian, arXiv:1407.8175.
- [48] C. Ciofi degli Atti and S. Simula, *Phys. Rev. C* **53**, 1689 (1996).
- [49] R. B. Wiringa, R. Schiavilla, Steven C. Pieper, and J. Carlson, *Phys. Rev. C* **89**, 024305 (2014).
- [50] E. D. Kuhnle, et al., *Phys. Rev. Lett.* **105**, 070402 (2010).
- [51] X.H. Li et al., in preparation (2014).
- [52] J. Dobaczewski, W. Nazarewicz, P.-G. Reinhard, *J. Phys. G: Nucl. Part. Phys.* **41**, 074001 (2014).
- [53] J. Piekarewicz, Wei-Chia Chen and F.J. Fattoyev, arXiv:1407.0911
- [54] Z.Chajeccki and Betty Tsang, private communications (2014).
- [55] B.A. Li, W.J. Guo and Z.Z. Shi in preparation (2014).
- [56] B.A. Li, C. B. Das, S. Das Gupta, C. Gale, *Nucl. Phys. A* **735**, 563 (2004).

Supplementary Information for: Kinetic symmetry energy of nucleonic matter with tensor correlations

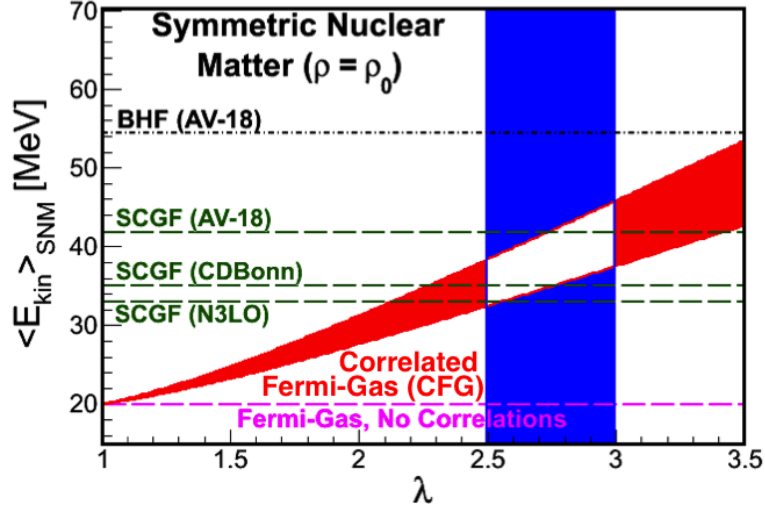


FIG. S1: The per-nucleon kinetic energy for symmetric nuclear matter calculated using the Correlated Fermi Gas (CFG) model (red band). The calculated kinetic energy is shown as a function of λ , the high-momentum tail cutoff parameter. The blue band shows the constraints on λ from the deuteron momentum distribution. The red band reflects the model uncertainties. Also shown are the results from the uncorrelated Fermi Gas model (dashed purple line), the Brueckner-Hartree-Fock (BHF) model using the AV-18 interaction [21], and the Self-Consistent Greens Function (SCGF) approach using the CDBonn, N3LO, AV18 and Nij1 interactions [23, 24].

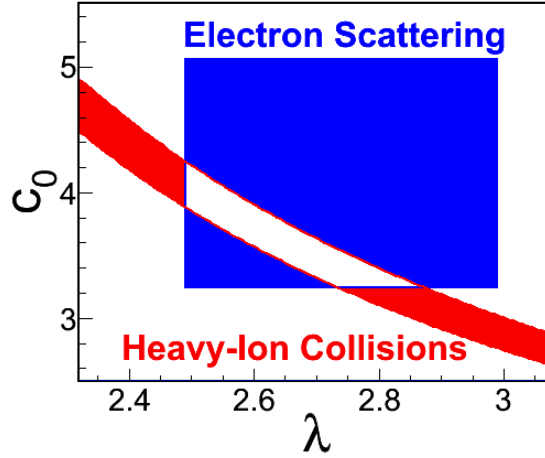


FIG. S2: The constraints on the width (λ) and strength (c_0) parameters of the Correlated Fermi Gas (CFG) model from electron scattering (blue box) and Sn-Sn collisions as described in the text (red band).